Supporting Information

Activatable carbocyanine dimers for photoacoustic and fluorescent detection of protease activity

Colman Moore[1], Raina M. Borum[1], Yash Mantri[2], Ming Xu[1], Pavla Fajtová[3], Anthony J. O'Donoghue[3], and Jesse V Jokerst[1,4,5*]

1. Department of Nanoengineering
2. Department of Bioengineering
3. Skaggs School of Pharmacy and Pharmaceutical Sciences
4. Materials Science and Engineering Program
5. Department of Radiology

University of California, San Diego. La Jolla, CA 92093. United States.
*jjokerst@eng.ucsd.edu

Table of Contents

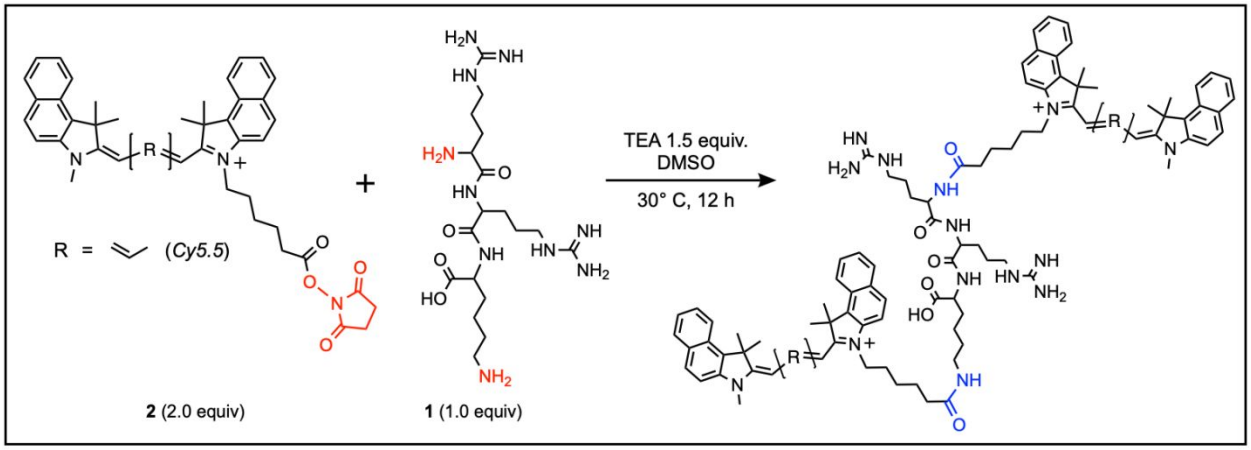

Scheme S1. Synthetic scheme for dye-peptide conjugates. For brevity, only the RRK peptide is illustrated. Succinimidyl ester activated dyes (Cy5.5-NHS) were reacted with the N-terminal amines and lysine side chains of the peptides (RRK, RRKRRK, RRKRRKRRK, GHK, GTSAVLQSGFRK) to form amide linkages.

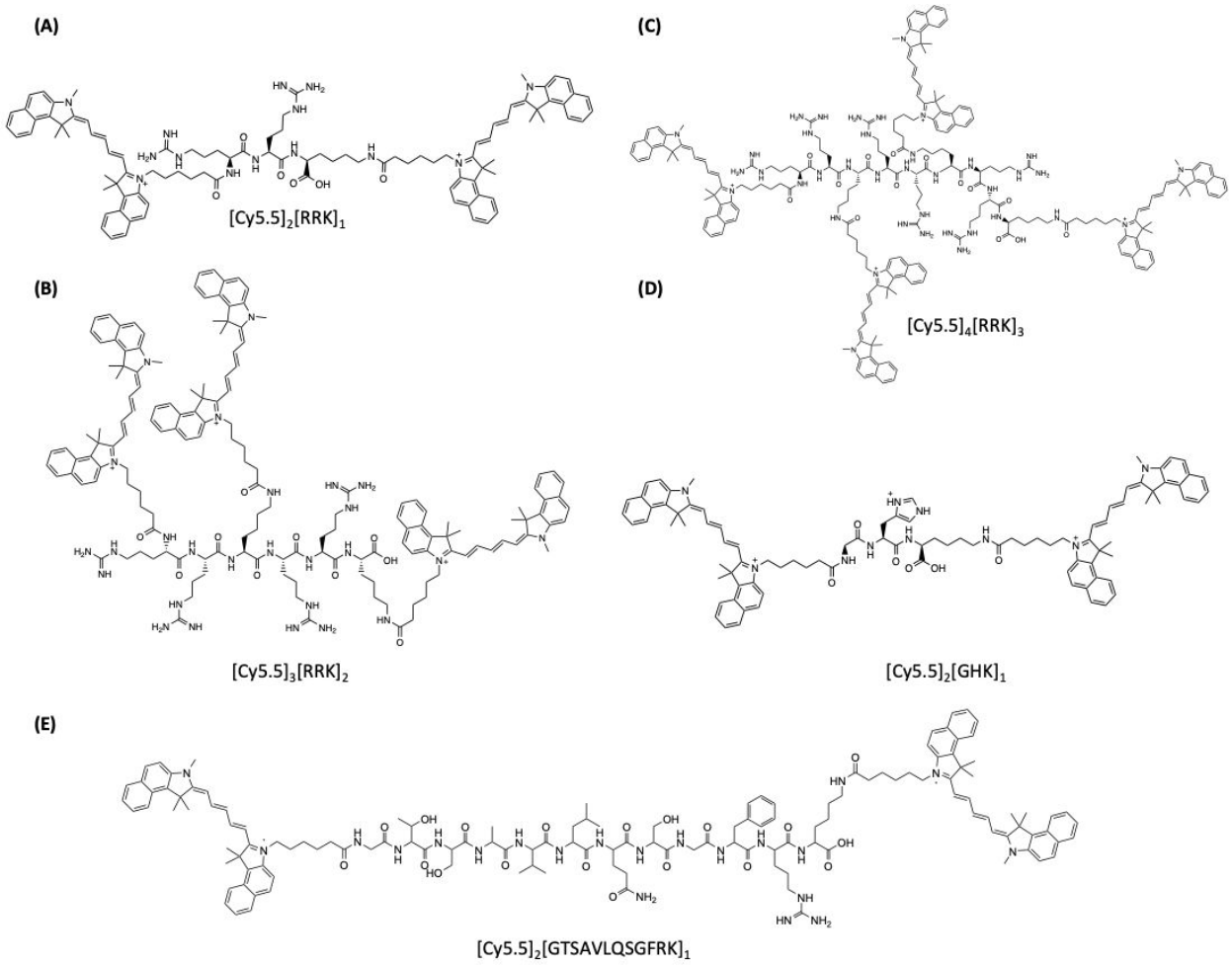

Figure S1. Structures of synthesized dye-peptide conjugates. (**A**) $[Cy5.5]_2[RRK]_1$, (**B**) $[Cy5.5]_3[RRK]_2$, (**C**) $[Cy5.5]_4[RRK]_3$, (**D**) $[Cy5.5]_2[GHK]_1$, and (**E**) $[Cy5.5]_2[GTSAVLQSGFRK]_1$.

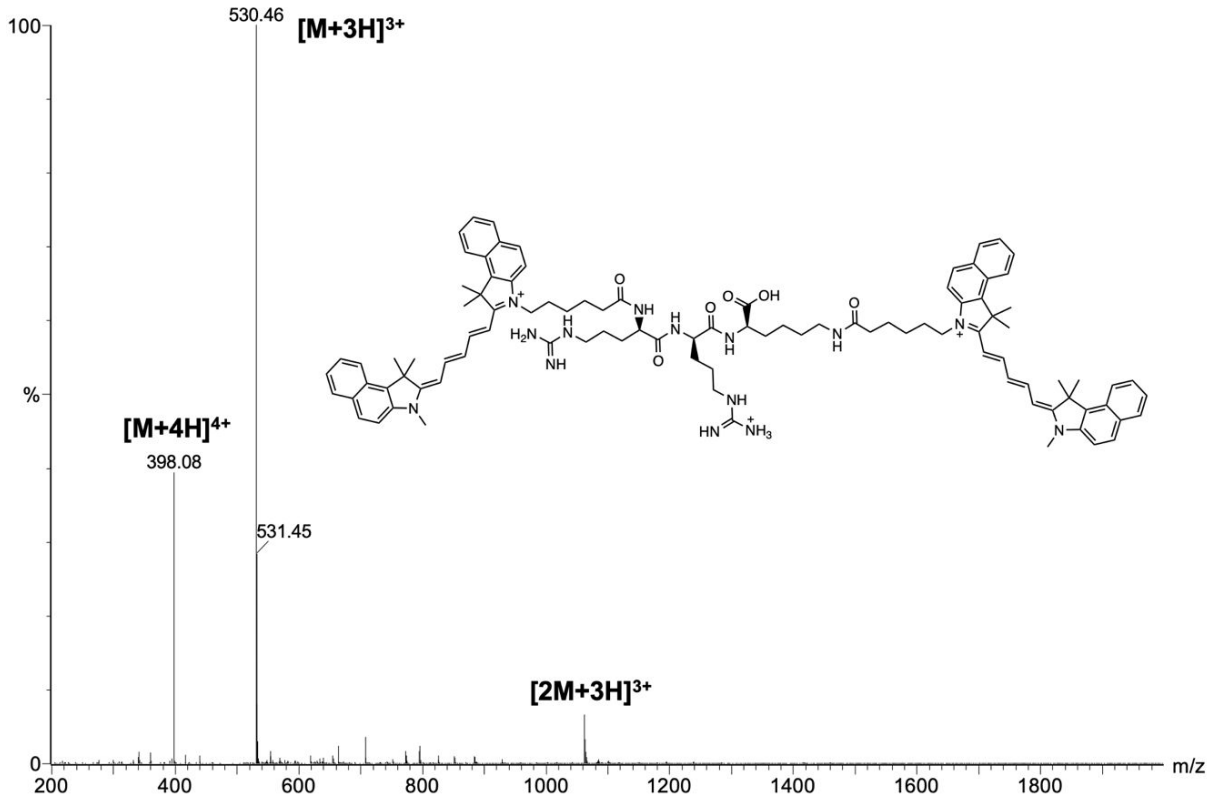

Figure S2. ESI-MS spectrum of $[Cy5.5]_2[RRK]_1$ in positive mode.

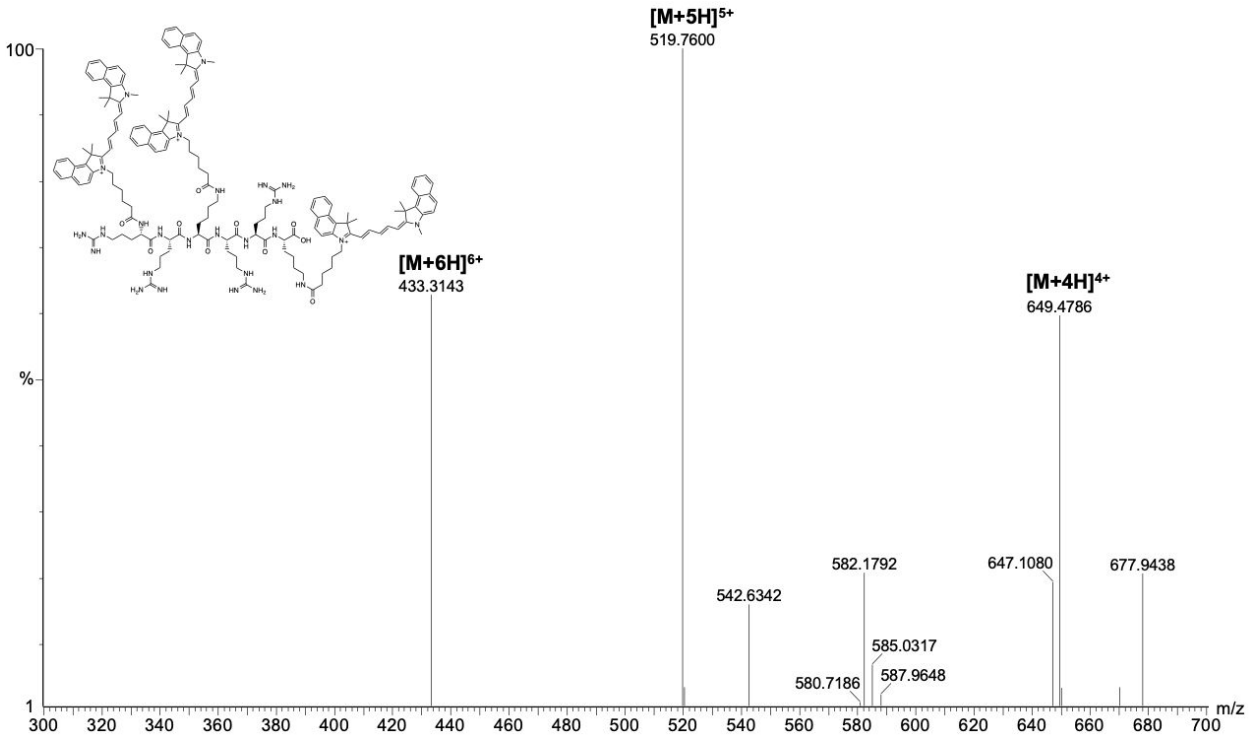

Figure S3. ESI-MS spectrum of $[Cy5.5]_3[RRK]_2$ in positive mode.

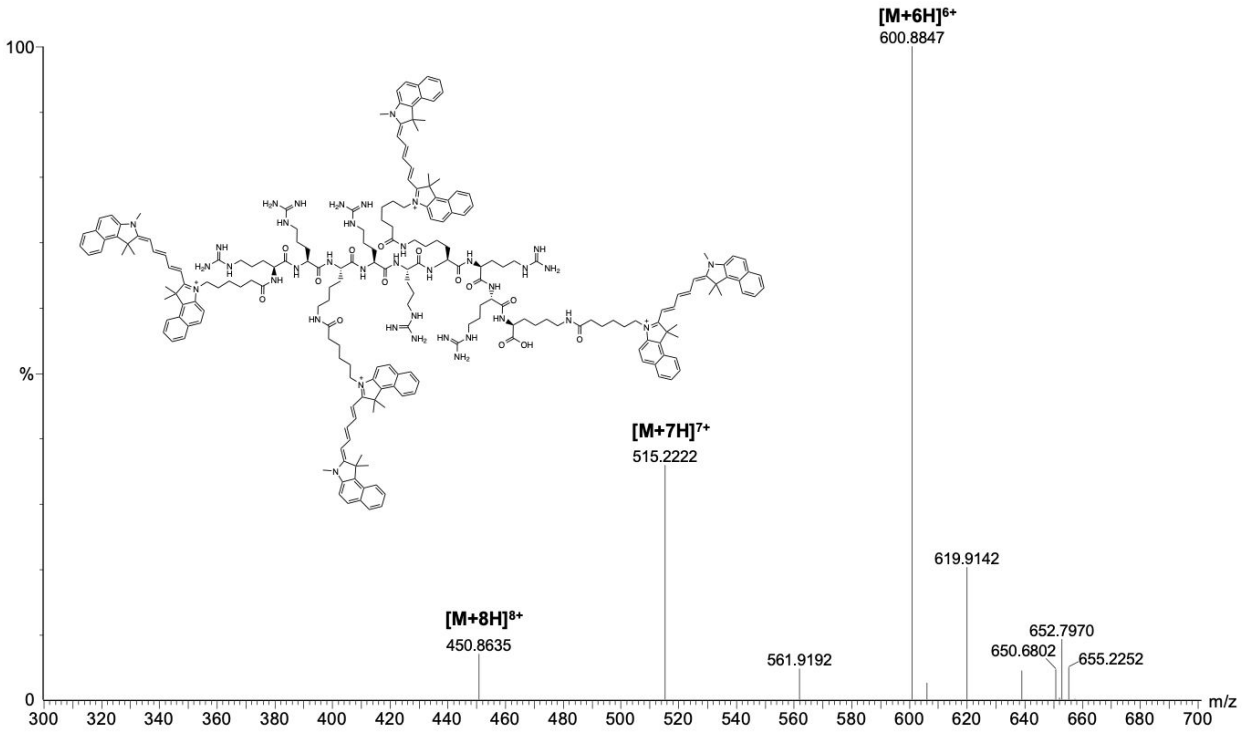

Figure S4. ESI-MS spectrum of $[Cy5.5]_4[RRK]_3$ in positive mode.

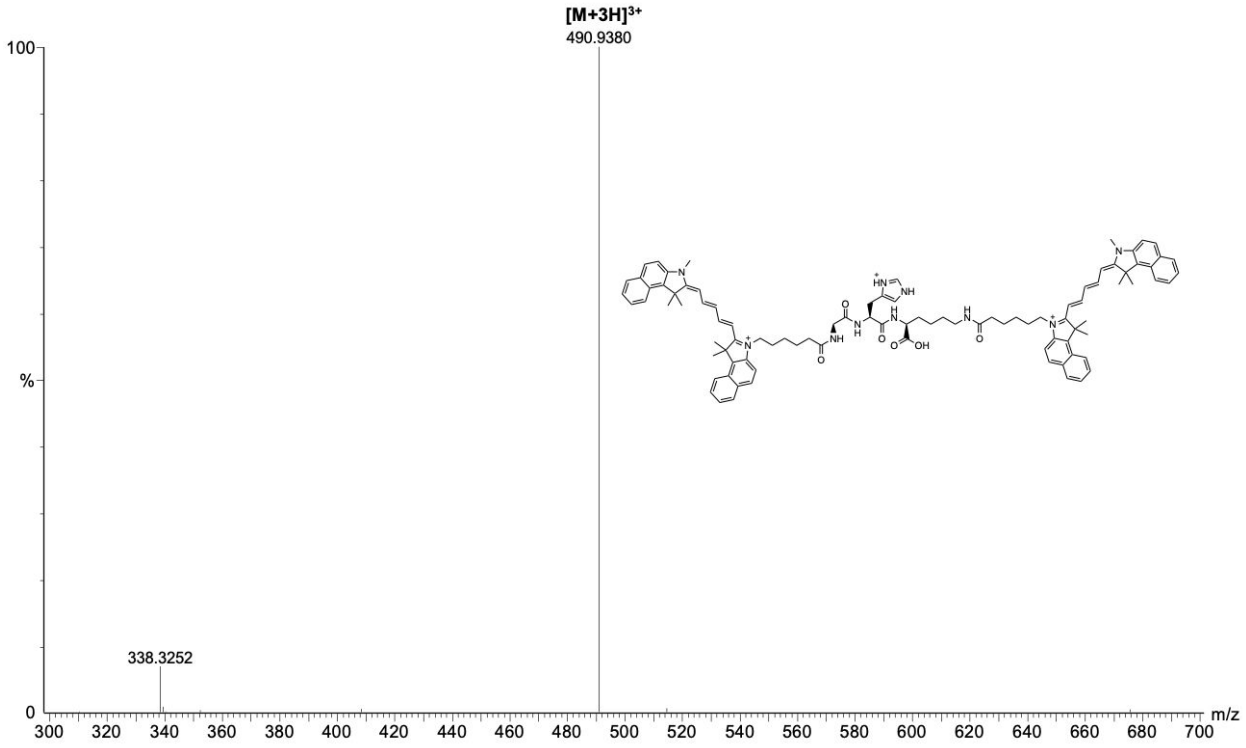

Figure S5. ESI-MS spectrum of $[Cy5.5]_2[GHK]_1$ in positive mode.

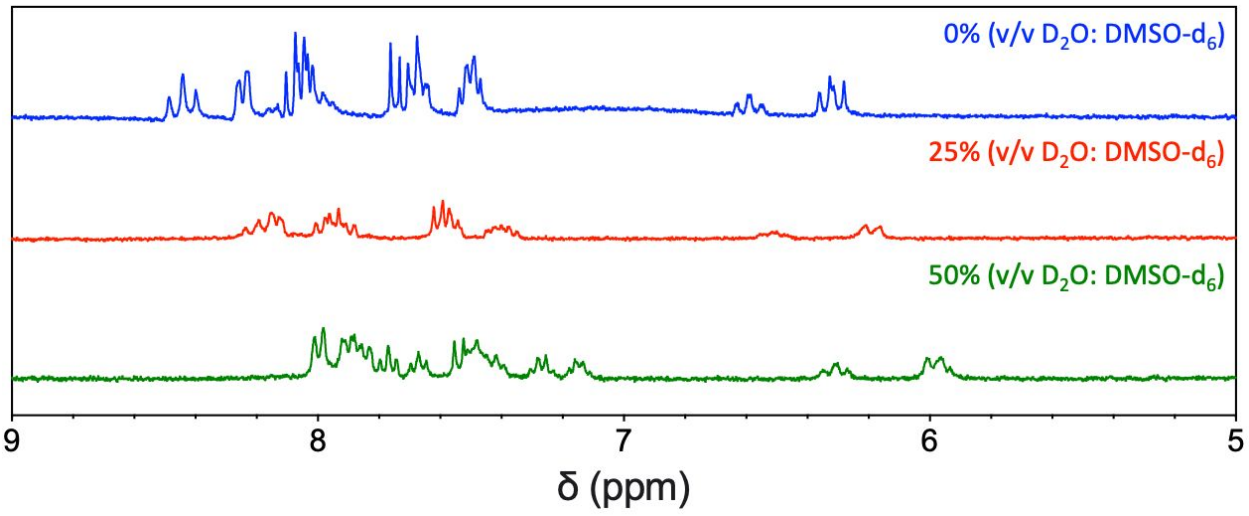

Figure S6. ^{1}H-NMR spectra (300 MHz) of $[Cy5.5]_2[RRK]_1$ in increasing ratios of D_2O/DMSO-d_6.

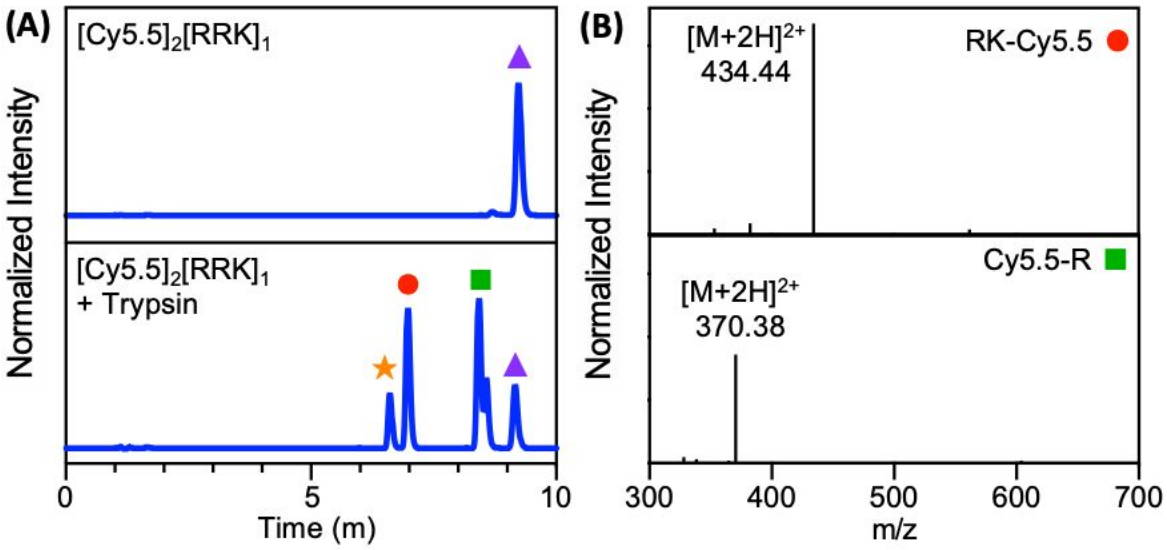

Figure S7. Liquid chromatograms and ESI-MS of $[Cy5.5]_2[RRK]_1$ before and after proteolysis. (**A**) $[Cy5.5]_2[RRK]_1$ (9 μM) without (top) and with (bottom) incubation in trypsin (100 nM) for 2 h at 37 °C in NH_5CO_3 (100 mM). Uncleaved probe eluted at 9 min. After proteolysis, new peaks were observed at 6.5 min, 6.9 min, and 8.3/8.5 min (collected as a single fraction). The column was an analytical-scale Shim-pack GIS C18 (5 μm) and the detection wavelength was 680 nm. The pumps were programmed with a binary gradient from 25 – 95% B (A: H_2O (0.05% TFA), B: MeCN (0.05% TFA)) over 45 min). (**B**) The C-terminal RK-Cy5.5 fragment was detected via ESI-MS in the 6.9-min fraction (expected: 434.27, observed: 434.44) and the N-terminal Cy5.5-R fragment was detected in the 8.3/8.5 min fraction (expected: 370.22, observed: 370.38).

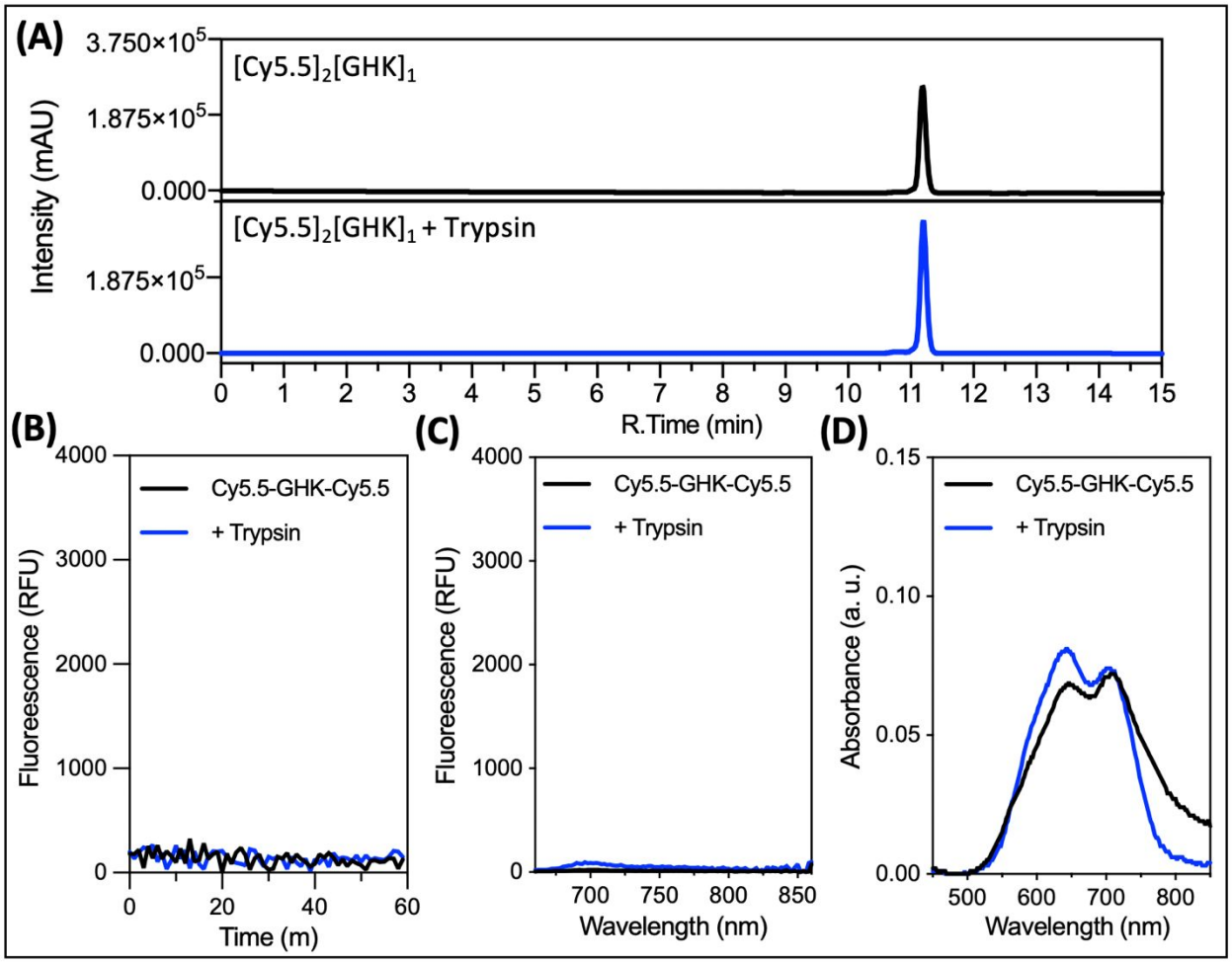

Figure S8. Liquid chromatograms and optical spectra of control sequence ($[Cy5.5]_2[GHK]_1$) before and after incubation with trypsin. (**A**) $[Cy5.5]_2[GHK]_1$ (2 µM) without (top) and with (bottom) incubation in trypsin (5 µM) for 2 h at 37 °C in NH_5CO_3 (100 mM). (**B**) Kinetic fluorescence measurements of $[Cy5.5]_2[GHK]$ with and without trypsin for 1 h (ex: 600 nm, em: 700 nm). (**C**) Fluorescence spectra recorded after 1 h (ex: 600 nm, em: 660 – 850 nm). (**D**) Absorbance spectra recorded after 1 h.

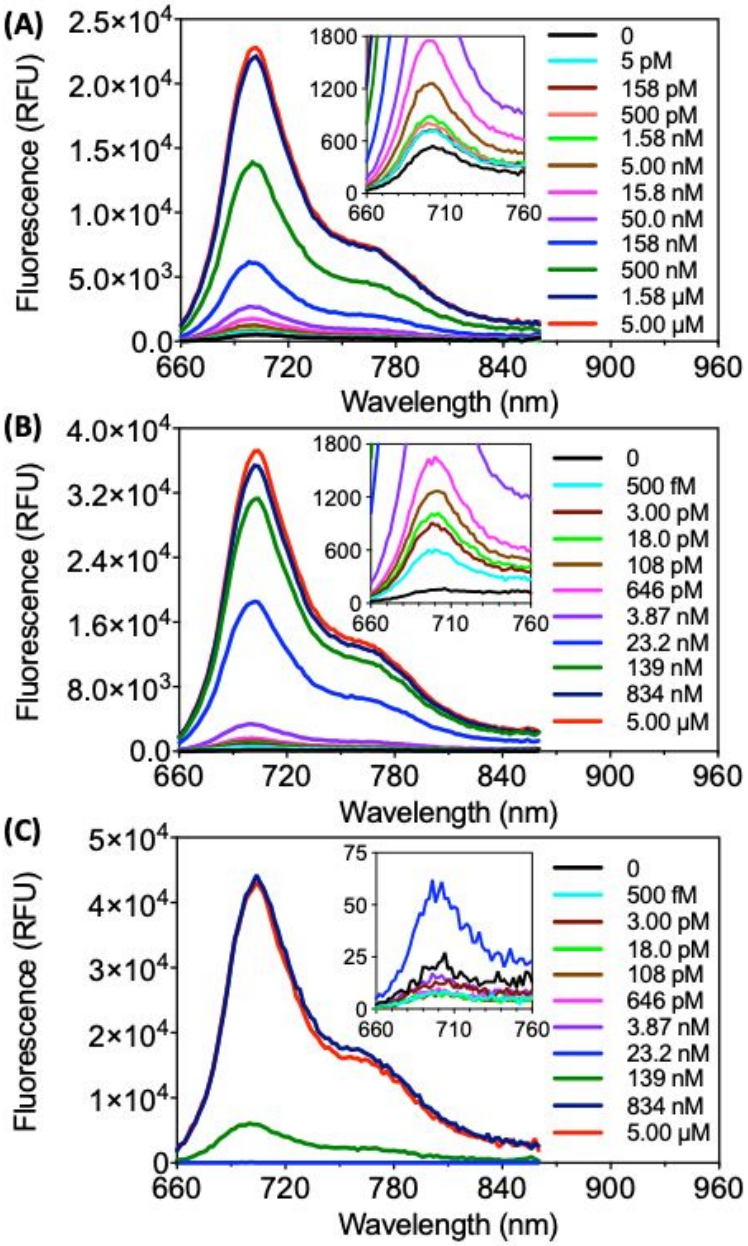

Figure S9. Representative fluorescence spectra for (A) $[Cy5.5]_2[RRK]_1$, (B) $[Cy5.5]_3[RRK]_2$, and (C) $[Cy5.5]_4[RRK]_3$ incubated with increasing trypsin concentrations. Probes were maintained at 7 µM and incubated with a trypsin gradient in 10 mM NH_4HCO_3 and 1% DMSO for 1 h at 37 ° C (ex: 600 nm).

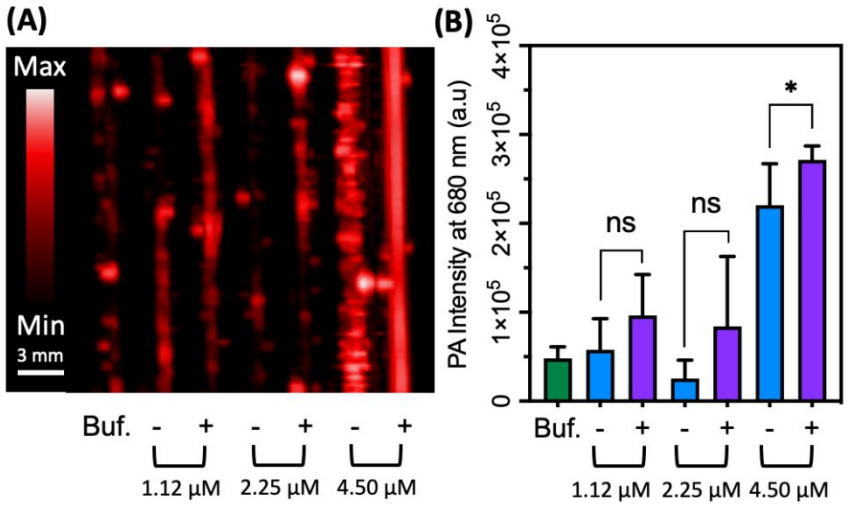

Figure S10. Photoacoustic imaging of $[Cy5.5]_2[RRK]_1$ cleavage at insufficient probe concentrations. (A) Photoacoustic image of $[Cy5.5]_2[RRK]_1$ at low concentrations (1 – 4.5 µM) before (-) and after (+) incubation with trypsin. (**B**) Quantitation of (A) via integrated pixel intensity. Asterisks denote significant difference (unpaired t-test, p-value < 0.0001, n = 8 regions of interest, error bars = SD).

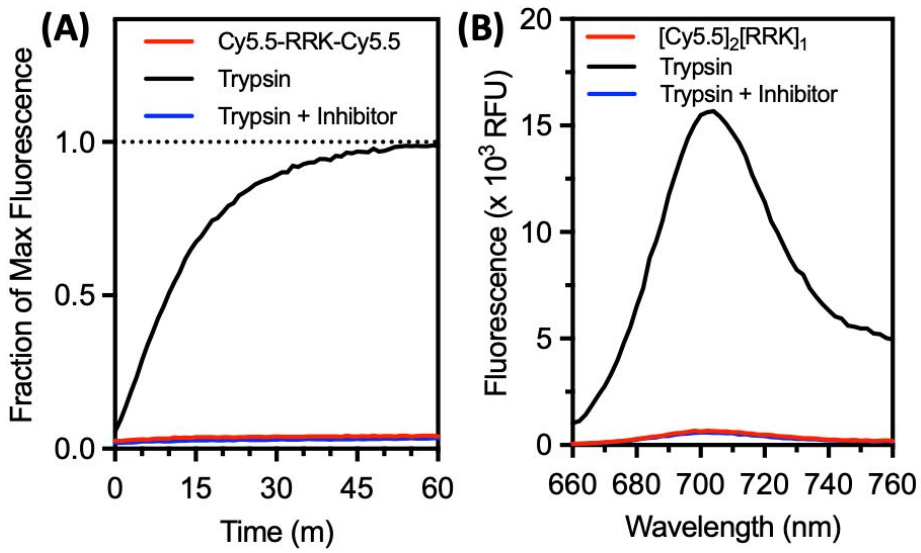

Figure S11. Fluorescent activation of $[Cy5.5]_2[RRK]_1$ following proteolytic cleavage by trypsin. (A) Fluorescence over time and (**B**) spectra of $[Cy5.5]_2[RRK]_1$ (7 μM) with trypsin (5 μM) and trypsin/inhibitor (50 μM leupeptin) after 1 h incubation in 100 mM NH_5CO_3 (1% DMSO) at 37 ° C.

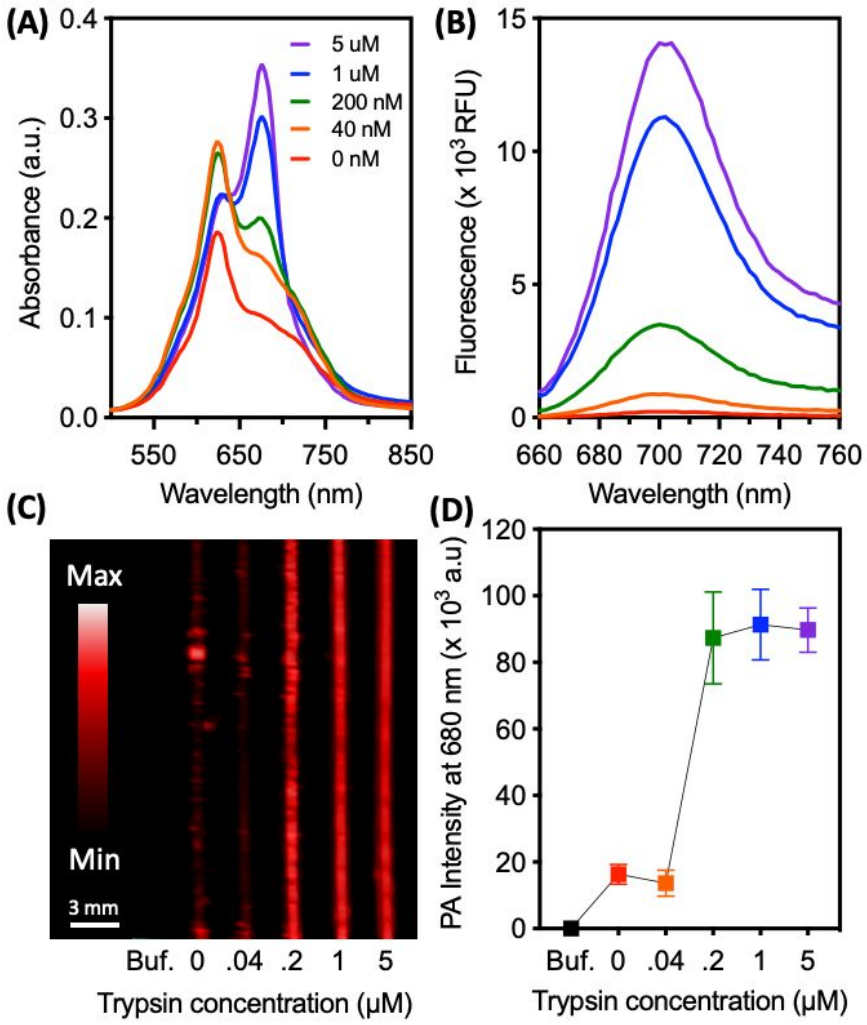

Figure S12. Photoacoustic sensitivity of $[Cy5.5]_2[RRK]_1$ to various trypsin concentrations. **(A)** Absorbance spectra of the dimer probe (7 μM) with 0 – 5 μM trypsin after 1 h incubation in 100 mM NH_5CO_3 (1% DMSO) at 37 ° C. As trypsin concentration increased, broadband absorption first increased, followed by an increase in the 680-nm peak and decrease in the 624-nm shoulder. (**B**) Fluorescence spectra of the samples (ex: 600 nm). (**C**) Single-wavelength photoacoustic image of the samples (ex: 680 nm). (**D**) Quantification of Panel C via integrated pixel density. Error bars = SD, n = 8 regions of interest.

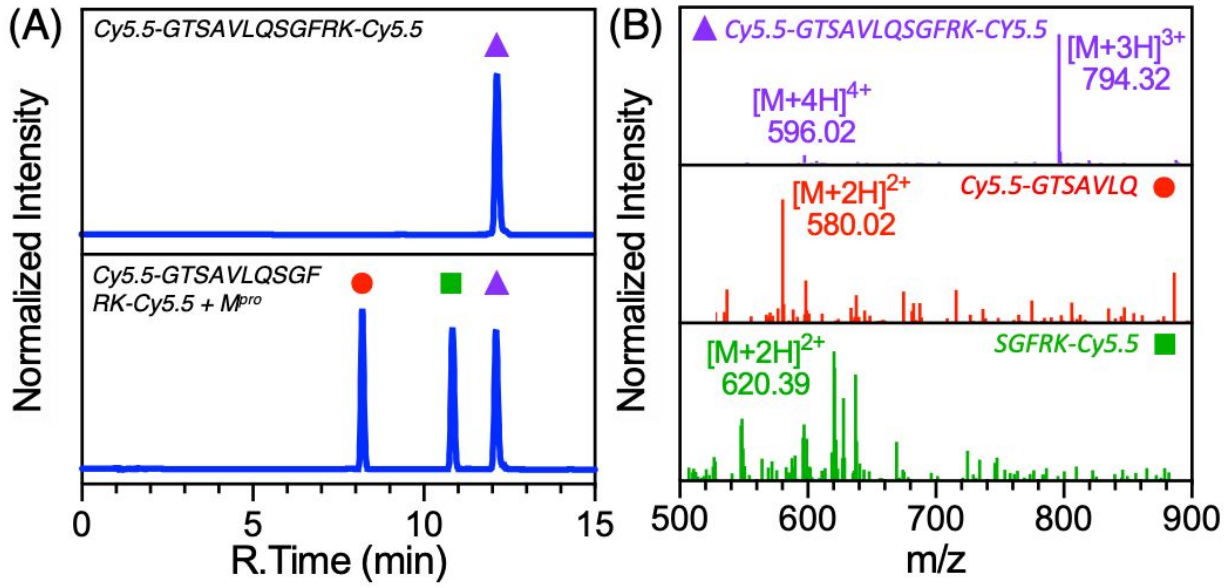

Figure S13. RP-HPLC and ESI-MS of M^{pro}-responsive cyanine-peptide conjugate $[Cy5.5]_2[GTSAVLQSGFRK]_1$. (A) Top: Liquid chromatogram of pure $[Cy5.5]_2[GTSAVLQSGFRK]_1$ in buffer (18 μM, 20 mM Tris, 1 mM DTT, pH 7.4). The retention time was 12.1 min. Bottom: Liquid chromatogram of $[Cy5.5]_2[GTSAVLQSGFRK]_1$ (18 μM) incubated with M^{pro} (100 nM) for 1 h at 37 ° C (20 mM Tris, 1 mM DTT, pH 7.4). The retention times were 8.1 min, 10.7 min, and 12.1 min. Samples were eluted at 1 mL/min with a 25-min gradient from 25% to 95% B (A: water (0.05% TFA), B: acetonitrile (0.05% TFA)). **(B)** ESI-MS of the fractions in Panel A. Fraction 12.1 min (uncleaved $[Cy5.5]_2[GTSAVLQSGFRK]_1$) expected $[M+3H]^{3+}$: 794.11, detected: 794.32, expected $[M+4H]^{4+}$: 595.83, detected: 596.02. Fraction 8.1 min (N-terminal fragment Cy5.5-GTSAVLQ) expected $[M+2H]^{2+}$: 620.34, detected: 620.39. Fraction 10.7 min (C-terminal fragment SGFRK-Cy5.5) expected $[M+2H]^{2+}$: 794.11, detected: 794.41.

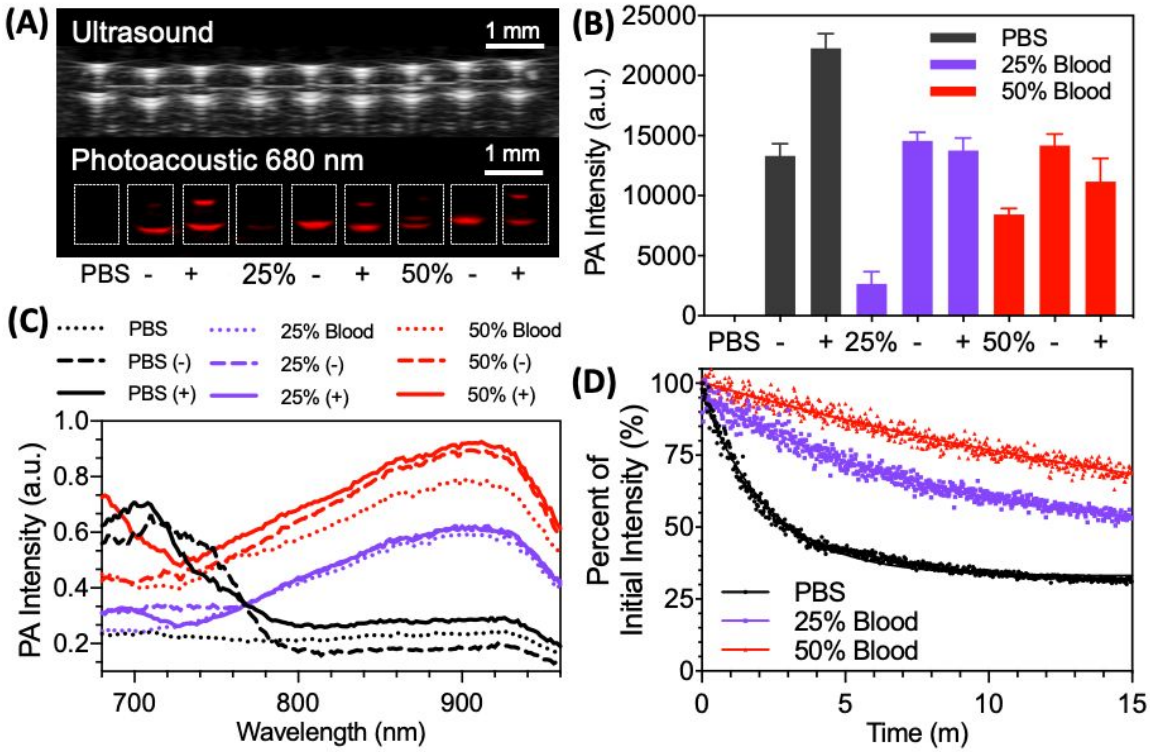

Figure S14. Photoacoustic signal and stability of the $[Cy5.5]_2[RRK]_1$ probe in blood. (A) Representative photoacoustic and ultrasound B-mode image of the probe in various matrices held in polyethylene capillary tubes (left to right): PBS, probe in PBS (-), probe/trypsin in PBS (+), 25% blood, probe in 25% blood (-), probe/trypsin in 25% blood (+), 50% blood, probe in 50% blood (-), probe/trypsin in 50% blood (+). Blood was diluted with PBS (v/v), [probe] = 30 μM, [trypsin] = 1 μM. **(B)** Average intensities from the B-mode images (dashed boxes = ROIs, n = 8 images) taken at different points along the length of the samples. Samples containing probe had significantly higher intensities than matrix alone (PBS, 25%, 50% blood). The 680-nm average intensity of cleaved probe was not statistically higher than uncleaved in 25% and 50% blood likely due to the strong absorption of hemoglobin. **(C)** Photoacoustic spectra of the samples in Panel A. Both uncleaved and cleaved probe in PBS (black) are spectrally unique from hemoglobin in blood (purple, red). In each matrix, cleaved probe (solid) is spectrally unique (680-nm enhancement) from uncleaved probe (dashed). **(D)** Photostability of cleaved probe in PBS, 25% blood, and 50% blood. Each sample was continuously imaged for 15 minutes—the PA intensity at each timepoint was normalized to its initial intensity. The probe intensity was reduced by 69%, 48%, and 30% in PBS, 25% blood, and 50% blood, respectively. Higher stability in blood was due to the increased absorption of light by hemoglobin.

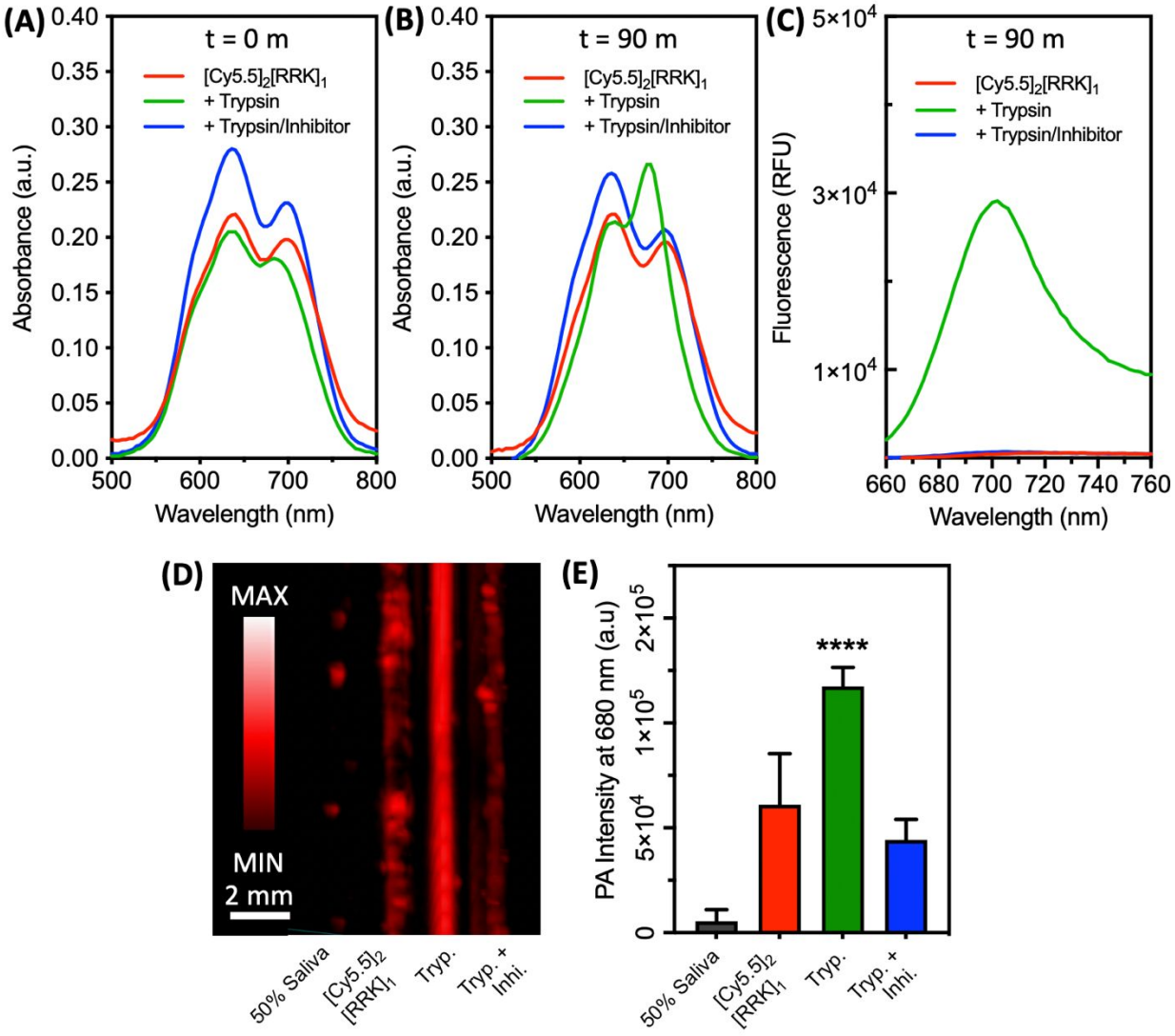

Figure S15. Photoacoustic imaging of $[Cy5.5]_2[RRK]_1$ cleavage by trypsin in 50% saliva. (A) Absorbance spectra of $[Cy5.5]_2[RRK]_1$ (7 μM) immediately after addition of trypsin (5 μM) and trypsin/inhibitor (50 μM leupeptin) in 50% pooled human saliva (v/v saliva: 100 mM NH_5CO_3). (**B**) Absorbance spectra after 90 min at 37 ° C. (**C**) Fluorescence spectra after 90 min at 37 ° C (ex: 600 nm). (**D**) Photoacoustic image of the samples at 680 nm. (**E**) Quantitation of (D) via integrated pixel density. Asterisks denote significant difference between $[Cy5.5]_2[RRK]_1$ and trypsin and trypsin with inhibitor (unpaired t-test, p-value < 0.0001, n = 8 regions of interest, error bars = SD).

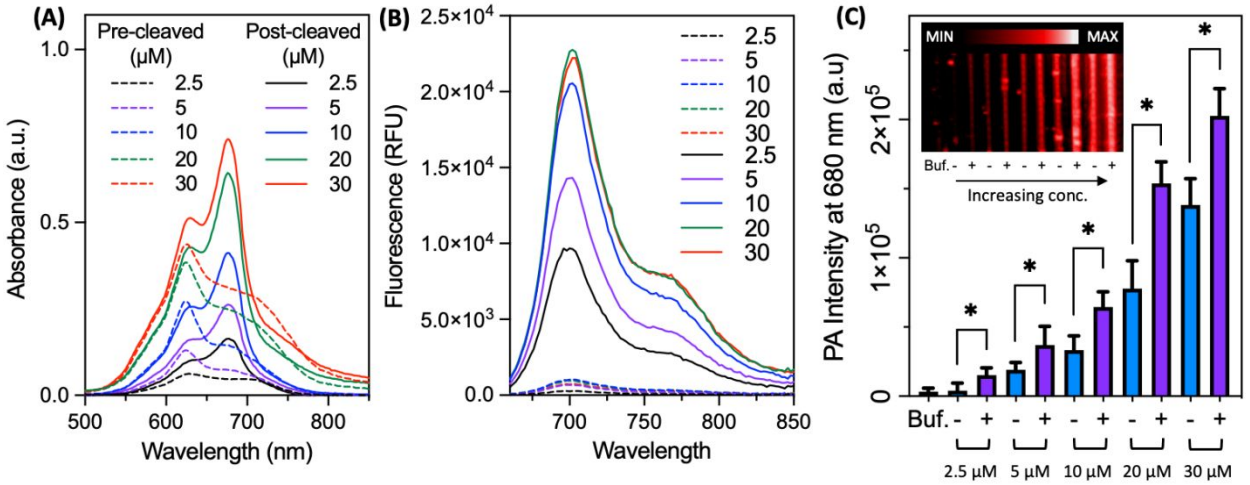

Figure S16. Optical and photoacoustic properties of uncleaved and cleaved $[Cy5.5]_2[RRK]_1$ at a range of probe concentrations. **(A)** Absorbance spectra of $[Cy5.5]_2[RRK]_1$ at 2.5, 5, 10, 20, and 30 μM before (dashed) and after (solid) incubation with trypsin (1 h, 5 μM trypsin, 37° C, NH_4HCO_3 buffer, 1% DMSO) reveal red shifts of the peak absorption at all concentrations. **(B)** Fluorescence spectra of the same samples before (dashed) and after (solid) incubation with trypsin (ex: 600 nm) show concentration-dependent enhancement. **(C)** Photoacoustic image (inset) and quantitation of the samples excited at 680 nm. All tested concentrations showed photoacoustic enhancement of cleaved probe (purple) relative to uncleaved (blue). Asterisks denote significant difference (unpaired t test, $p < 0.05$, error bars = S.D. of eight regions of interest per sample).

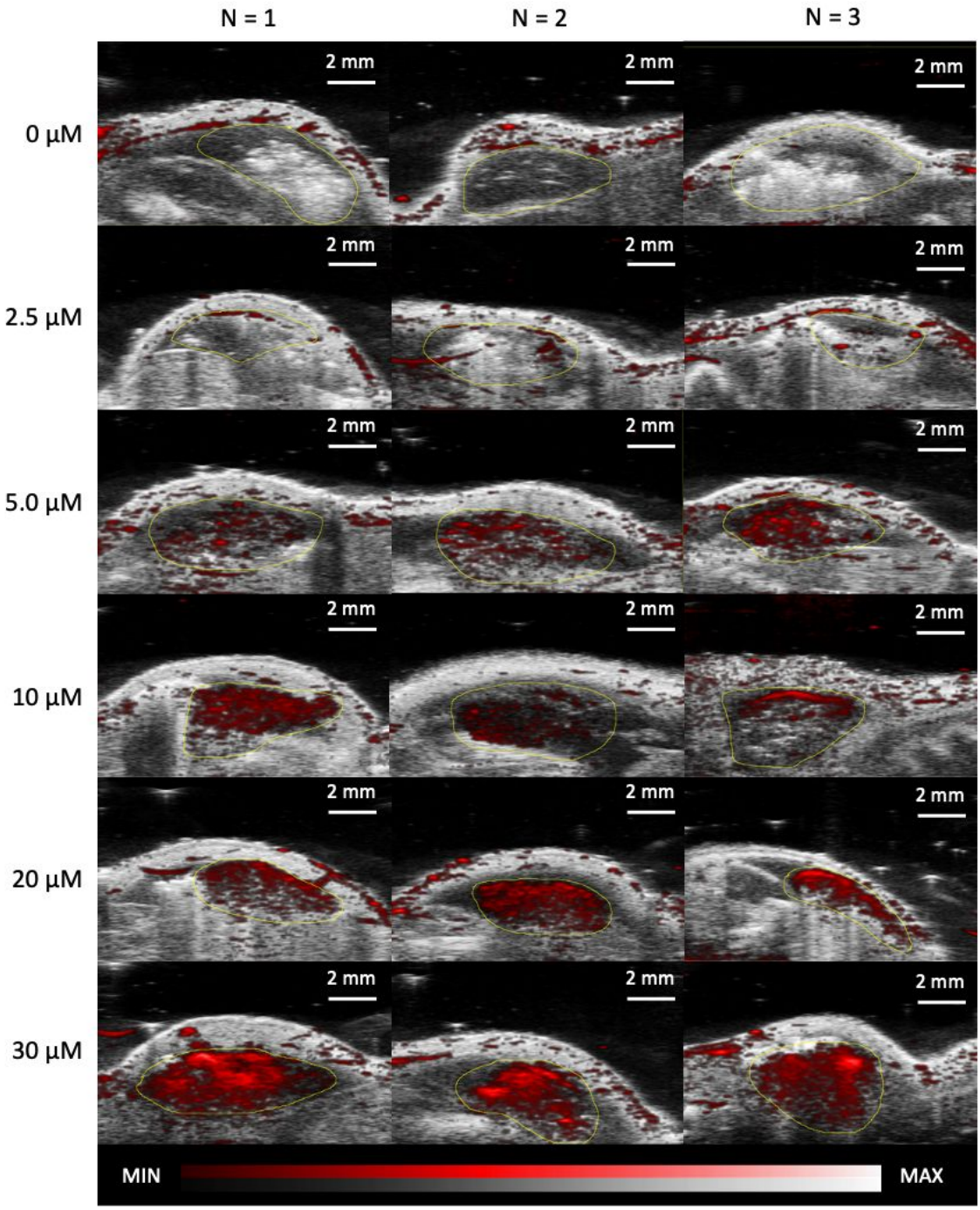

Figure S17. Individual photoacoustic-ultrasound images of subcutaneous injections of $[Cy5.5]_2[RRK]_1$ in nude mice. The injection volume was the same for each concentration (100 µL of probe in 50% (v/v) Matrigel). However, normal variations in the mice and transducer coupling contributed to differences in the apparent size (and cross-sectional area) of the injection sites. ROIs were drawn in ImageJ for each injection area (yellow) based on the ultrasound image. Because the ROIs had different areas, we calculated the raw integrated density of the PA signal for each ROI and used these values for analysis in Fig. 7. Unlike mean pixel intensity, the raw integrated density is not skewed by pixels with zero intensity, making it appropriate for comparison of ROIs with minor differences in area.